Supplementary Material

I. DERIVATION OF THE EFFECTIVE MODEL

We consider the microscopic model which describes the interaction of a single particle of mass m_I with a weakly interacting gas of bosons of mass m_B. We assume that the interactions between the particles are described by contact interactions. This approximation is valid for the description of ultracold gases close to a broad inter-species Feshbach resonance [1]. The Hamiltonian reads

$$\hat{H} = \sum_{\mathbf{k}} \epsilon^B_{\mathbf{k}} \hat{a}^\dagger_{\mathbf{k}} \hat{a}_{\mathbf{k}} + \frac{g_{BB}}{2} \sum_{\mathbf{k}\mathbf{k}'\mathbf{q}} \hat{a}^\dagger_{\mathbf{k}+\mathbf{q}} \hat{a}^\dagger_{\mathbf{k}'-\mathbf{q}} \hat{a}_{\mathbf{k}} \hat{a}_{\mathbf{k}'} + \sum_{\mathbf{k}} \epsilon^I_{\mathbf{k}} \hat{d}^\dagger_{\mathbf{k}} \hat{d}_{\mathbf{k}} + g_\Lambda \sum_{\mathbf{k}\mathbf{k}'\mathbf{q}} \hat{a}^\dagger_{\mathbf{k}+\mathbf{q}} \hat{a}_{\mathbf{k}} \hat{d}^\dagger_{\mathbf{k}'-\mathbf{q}} \hat{d}_{\mathbf{k}'} \quad (1)$$

where $\hat{a}^\dagger_{\mathbf{k}}$ and $\hat{d}^\dagger_{\mathbf{k}}$ are the creation operators that describe the bosonic host particles and an impurity with the corresponding dispersion relations $\epsilon^B_{\mathbf{k}} = \frac{k^2}{2m_B}$ and $\epsilon^I_{\mathbf{k}} = \frac{k^2}{2m_I}$. The parameters of the contact interaction (bare interaction) are given by the coefficient g_Λ for the interaction between the host particles and the impurity and g_{BB} for the interaction among the host particles. We allow for the general case of a mass imbalanced system where the mass of the bosonic field m_B and the mass of the impurity m_I are not fixed to be equal.

We account for the macroscopic occupation of the $\mathbf{k} = 0$ mode within the Bogoliubov approximation [2]. Following the corresponding truncation of the Hamiltonian on the quadratic level in the bosonic creation and annihilation operators we diagonalize the purely bosonic part of the Hamiltonian by a unitary Bogoliubov rotation

$$a_{\mathbf{k}} = u_{\mathbf{k}} b_{\mathbf{k}} - v_{\mathbf{k}} b^\dagger_{-\mathbf{k}}. \quad (2)$$

Here the coefficients are given by $u^2_{\mathbf{k}} = \frac{1}{2}\left(\frac{\varepsilon_{\mathbf{k}}+g_{\mathrm{BB}}n}{\omega_{\mathbf{k}}} + 1\right)$, $v^2_{\mathbf{k}} = \frac{1}{2}\left(\frac{\varepsilon_{\mathbf{k}}+g_{\mathrm{BB}}n}{\omega_{\mathbf{k}}} - 1\right)$. This transformation introduces the Bogoliubov quasiparticles with dispersion relation $\omega_{\mathbf{k}}$ which are created by the operators $b^\dagger_{\mathbf{k}}$. Reexpressing the resulting Hamiltonian in explicit impurity coordinates yields the Hamiltonian (1) given in the main text.

In order to take advantage of momentum conservation we perform a canonical transformation to the so-called polaron frame using $\hat{S} = e^{i\hat{\mathbf{R}}\hat{\mathbf{P}}_B}$ where $\hat{\mathbf{P}}_B = \sum_{\mathbf{k}} \mathbf{k} \hat{b}^\dagger_{\mathbf{k}} \hat{b}_{\mathbf{k}}$ is the total momentum operator of the bosons. The operator $\hat{S}$ transforms the momentum of the impurity and bosonic operators in the following way

$$\hat{S}^{-1}\hat{\mathbf{P}}\hat{S} = \hat{\mathbf{P}} - \sum_{\mathbf{k}} \mathbf{k} \hat{b}^\dagger_{\mathbf{k}} \hat{b}_{\mathbf{k}} \quad (3)$$
$$\hat{S}^{-1}\hat{b}_{\mathbf{k}}\hat{S} = \hat{b}_{\mathbf{k}} e^{-i\hat{\mathbf{R}}\mathbf{k}}.$$

Applying this transformation to the Hamiltonian (1) of the main text, $\hat{\mathcal{H}} = \hat{S}^{-1}\hat{H}\hat{S}$, we obtain

$$\hat{\mathcal{H}} = = g_\Lambda n + \frac{1}{2m_I}\left(\hat{\mathbf{P}} - \sum_{\mathbf{k}} \mathbf{k} \hat{b}^\dagger_{\mathbf{k}} \hat{b}_{\mathbf{k}}\right)^2 + \sum_{\mathbf{k}} \omega_{\mathbf{k}} \hat{b}^\dagger_{\mathbf{k}} \hat{b}_{\mathbf{k}} + \frac{g_\Lambda \sqrt{n}}{L^{d/2}} \sum_{\mathbf{k}} W_{\mathbf{k}} \left(\hat{b}^\dagger_{\mathbf{k}} + \hat{b}_{-\mathbf{k}}\right) + \frac{g_\Lambda}{L^d} \sum_{\mathbf{k}\mathbf{k}'} V^{(1)}_{\mathbf{k}\mathbf{k}'} b^\dagger_{\mathbf{k}} b_{\mathbf{k}'} + \frac{g_\Lambda}{L^d} \sum_{\mathbf{k}\mathbf{k}'} V^{(2)}_{\mathbf{k}\mathbf{k}'} \left(b^\dagger_{\mathbf{k}} b^\dagger_{\mathbf{k}'} + b_{-\mathbf{k}} b_{-\mathbf{k}'}\right). \quad (4)$$

Since $\hat{\mathbf{P}}$ now commutes with the Hamiltonian, the Hilbert space of the Hamiltonian $\hat{\mathcal{H}}$ (4) becomes a direct product of the sub-spaces characterized by the total momentum of the system.

II. DERIVATION OF THE SADDLE POINT SOLUTION

In this section we derive the saddle point solution of the equations of motions of the parameters in Eq. (5) of the main text. We set the left hand side of the first equation to zero and obtain the following equation which defines the saddle point

$$0 = g_\Lambda \sqrt{n} W_{\mathbf{k}} + \Omega_{\mathbf{k}} \beta_{\mathbf{k}} + \frac{1}{2} g_\Lambda W_{\mathbf{k}} \sum_{\mathbf{k}'} W_{\mathbf{k}'} \left(\beta_{\mathbf{k}'} + \beta^*_{\mathbf{k}'}\right) + \frac{1}{2} g_\Lambda W^{-1}_{\mathbf{k}} \sum_{\mathbf{k}'} W^{-1}_{\mathbf{k}'} \left(\beta_{\mathbf{k}'} - \beta^*_{\mathbf{k}'}\right). \quad (5)$$

Here $\Omega_{\mathbf{k}} = \omega_{\mathbf{k}} + \frac{\mathbf{k}^2}{2M} - \frac{\mathbf{k}}{M}(\mathbf{P} - \mathbf{P}_B)$, $\mathbf{P}_B = \sum_{\mathbf{k}} \mathbf{k} |\beta_{\mathbf{k}}|^2$, and $\mathbf{P}$ denotes the total system momentum. The real and imaginary parts of the coherent amplitudes $\beta_{\mathbf{k}}$ can be expressed as

$$\mathrm{Re}\beta_{\mathbf{k}} = -g_\Lambda W_{\mathbf{k}} \frac{\sqrt{n} + \sum_{\mathbf{k}'} W_{\mathbf{k}'} \mathrm{Re}\beta_{\mathbf{k}'}}{\Omega_{\mathbf{k}}}, \quad (6)$$
$$\mathrm{Im}\beta_{\mathbf{k}} = -g_\Lambda W^{-1}_{\mathbf{k}} \frac{\sum_{\mathbf{k}'} W^{-1}_{\mathbf{k}'} \mathrm{Im}\beta_{\mathbf{k}'}}{\Omega_{\mathbf{k}}}.$$

The first equation allows for an analytical solution which is found by a multiplication with $W_{\mathbf{k}}$, a summation over all modes and expressing the problem in terms of the averaged quantity $\chi = \sum_{\mathbf{k}} W_{\mathbf{k}} \mathrm{Re}\beta_{\mathbf{k}}$. After some algebra one obtains

$$\mathrm{Re}\beta_{\mathbf{k}} = -\frac{\sqrt{n} W_{\mathbf{k}}}{\Omega_{\mathbf{k}}} \frac{1}{g^{-1}_\Lambda + \sum_{\mathbf{k}} \frac{W^2_{\mathbf{k}}}{\Omega_{\mathbf{k}}}}. \quad (7)$$

The microscopic interaction strength g_Λ is related to the impurity-boson scattering length a_{IB} by the zero-momentum limit of the Lippmann-Schwinger equation which yields

$$a^{-1}_{IB} = \frac{2\pi}{\mu_{\mathrm{red}}} g^{-1}_\Lambda + 4\pi \sum_{\mathbf{k}}^{\Lambda} \frac{1}{\mathbf{k}^2} \quad (8)$$

where Λ denotes a high-momentum cutoff which can be taken to infinity. Upon insertion into Eq. (7) one obtains

$$\mathrm{Re}\beta_{\mathbf{k}} = -\frac{2\pi}{\mu_{\mathrm{red}}} \frac{1}{a^{-1}_{IB} - a^{-1}_+} \frac{\sqrt{n} W_{\mathbf{k}}}{\omega_{\mathbf{k}} + \frac{\mathbf{k}^2}{2M} - \frac{\mathbf{k}}{M}(\mathbf{P} - \mathbf{P}_B)} \quad (9)$$

where we defined a_+^{-1} as

$$a_+^{-1} = \frac{2\pi}{\mu_{\rm red}} \sum_{\mathbf{k}} \left(\frac{2\mu_{\rm red}}{\mathbf{k}^2} - \frac{W_{\mathbf{k}}^2}{\omega_{\mathbf{k}} + \frac{\mathbf{k}^2}{2M} - \frac{\mathbf{k}}{M}(\mathbf{P}-\mathbf{P}_B)} \right). \quad (10)$$

The second equation has the trivial solution $\mathrm{Im}\beta_{\mathbf{k}} = 0$.

After the coherent amplitudes are expressed in terms of the inverse scattering length, a self-consistent procedure for the determination of a_+^{-1} and the total momentum of the phonons can be set up. To this end we substitute the Eq. (9) into the total momentum of the phonons, $\mathbf{P}_B = \sum_{\mathbf{k}} \mathbf{k} |\beta_k|^2$, and obtain the expression

$$\mathbf{P}_B = \left(\frac{2\pi\mu_{\rm red}^{-1}\sqrt{n}}{a_{IB}^{-1} - a_+^{-1}} \right)^2 \sum_k \frac{\mathbf{k} W_{\mathbf{k}}^2}{\left(\omega_{\mathbf{k}} + \frac{\mathbf{k}^2}{2M} - \frac{\mathbf{k}}{M}(\mathbf{P}-\mathbf{P}_B)\right)^2}. \quad (11)$$

The self-consistent solution of Eqs. (10) and (11) allows to find the saddle point for given initial conditions, a_{IB} and $\mathbf{P}$. Finally, the energy is obtained as expectation value of the Hamiltonian, given by Eq. (1) of the main text, in this state. After some algebra one obtains the expression for energy

$$E_{\rm pol}(\mathbf{P}) = \frac{\mathbf{P}^2 - \mathbf{P}_B^2}{2M} + \frac{2\pi}{\mu_{\rm red}} \frac{n}{a_{IB}^{-1} - a_0^{-1}}.$$

III. DERIVATION OF THE ENERGY OF THE BOUND STATES

In this section we provide the derivation of the bound state energy. We propose the wave-function which accounts for a single Bogoliubov excitation above the polaron state $\left|\Psi_{\rm pol}\right\rangle$

$$\left|\Psi'(t)\right\rangle = \sum_{\mathbf{k}} \gamma_{\mathbf{k}}(t) \hat{b}_{\mathbf{k}}^\dagger \left|\Psi_{\rm pol}\right\rangle. \quad (12)$$

The polaron state in the Lee-Low-Pines frame, i.e. after the transformation with $\hat{S}$, can be represented as a displacement operator $\hat{U}_{\rm pol}^\dagger[\beta_{\mathbf{k}}] = \exp\left(\sum_{\mathbf{k}} \beta_{\mathbf{k}} \hat{b}_{\mathbf{k}}^\dagger - \text{h.c.}\right)$ acting on the vacuum state, $\left|\Psi_{\rm pol}\right\rangle = \hat{U}_{\rm pol}^\dagger\left[\beta_{\mathbf{k}}^{\rm pol}\right]|0\rangle$. Here the $\beta_{\mathbf{k}}^{\rm pol}$ are defined by Eq. (9) in the previous section of the SM. After some algebra we can rewrite the state $|\Psi'(t)\rangle$ in the form

$$\left|\Psi'(t)\right\rangle \equiv \hat{U}_{\rm pol}^\dagger\left[\beta_{\mathbf{k}}^{pol}\right]\left(\gamma_0(t) + \sum_{\mathbf{k}} \gamma_{\mathbf{k}}(t)\hat{b}_{\mathbf{k}}^\dagger\right)|0\rangle \quad (13)$$

where $\gamma_0(t) = \sum_{\mathbf{k}} \gamma_{\mathbf{k}}(t)\beta_{\mathbf{k}}^{\rm pol}$. We calculate the Lagrangian of the system with respect to this state, $\mathcal{L} = \langle\Psi'(t)| \, i\partial_t - \hat{\mathcal{H}} \, |\Psi'(t)\rangle$, and obtain the equations of motion for the parameters of the wave-function (12)

$$i\partial_t \gamma_0(t) = E_{\rm pol}\gamma_0(t), \quad (14)$$

$$i\partial_t \gamma_{\mathbf{k}}(t) = \left(E_{\rm pol} + \Omega_{\mathbf{k}}\right)\gamma_{\mathbf{k}}(t) + \frac{g_\Lambda}{2}\sum_{\mathbf{k}'}\left(W_{\mathbf{k}}W_{\mathbf{k}'} + W_{\mathbf{k}}^{-1}W_{\mathbf{k}'}^{-1}\right)\gamma_{\mathbf{k}'}(t).$$

The first equation can be solved trivially assuming $\gamma_0(t) = 0$. This solution implies that the bound state solution is orthogonal to the polaron state. We are searching for a solution of these equations of motion such that the parameters $\gamma_{\mathbf{k}}(t)$ of the wave-function are time evolving with frequency ω, $\gamma_k \propto e^{-i\omega t}$. To this end we transform the second line of Eq. (14) to the frequency domain and find

$$\gamma_{\mathbf{k}}(\omega) = \frac{g_\Lambda}{2}\frac{W_{\mathbf{k}}}{\omega - E_{\rm pol} - \Omega_{\mathbf{k}}}\sum_{\mathbf{k}'} W_{\mathbf{k}'}\gamma_{\mathbf{k}'}(\omega) \quad (15)$$

$$+ \frac{g_\Lambda}{2}\frac{W_{\mathbf{k}}^{-1}}{\omega - E_{\rm pol} - \Omega_{\mathbf{k}}}\sum_{\mathbf{k}'} W_{\mathbf{k}'}^{-1}\gamma_{\mathbf{k}'}(\omega).$$

Multiplying by $W_{\mathbf{k}}$ or $W_{\mathbf{k}}^{-1}$ and summing over over the momentum we obtain the following matrix equation,

$$\begin{pmatrix} 1 - \frac{g_\Lambda}{2}\sum_{\mathbf{k}}\frac{W_{\mathbf{k}}^2}{\omega - E_{\rm pol} - \Omega_{\mathbf{k}}} & -\frac{g_\Lambda}{2}\sum_{\mathbf{k}}\frac{1}{\omega - E_{\rm pol} - \Omega_{\mathbf{k}}} \\ -\frac{g_\Lambda}{2}\sum_{\mathbf{k}}\frac{1}{\omega - E_{\rm pol} - \Omega_{\mathbf{k}}} & 1 - \frac{g_\Lambda}{2}\sum_{\mathbf{k}}\frac{W_{\mathbf{k}}^{-2}}{\omega - E_{\rm pol} - \Omega_{\mathbf{k}}} \end{pmatrix}$$
$$\otimes \begin{pmatrix} \sum_{\mathbf{k}} W_{\mathbf{k}}\gamma_{\mathbf{k}}(\omega) \\ \sum_{\mathbf{k}} W_{\mathbf{k}}^{-1}\gamma_{\mathbf{k}}(\omega) \end{pmatrix} = 0. \quad (16)$$

This equation has a nontrivial solution if and only if the determinant of the matrix is equal to zero. Neglecting terms that are vanishing in the limit $\Lambda \to \infty$, $\sim \Lambda^{-2}$, we obtain the following equation for the eigenenergy ω of the bound state

$$1 - \frac{g_\Lambda}{2}\sum_{\mathbf{k}}\frac{W_{\mathbf{k}}^2 + W_{\mathbf{k}}^{-2}}{\omega - E_{\rm pol} - \Omega_{\mathbf{k}}} = 0. \quad (17)$$

Using the Lippmann-Schwinger equation, given by Eq. (2) of the main text, we recast Eq. (17) in the form of Eq. (7) of the main text. This simple analysis agrees with the features below the polaron branch in the absorption spectrum as shown in Fig. 1.

IV. COMPARISON WITH OTHER APPROACHES

In this section we compare the results for the spectral function $A(\omega)$ of the Bose polaron in the vicinity of a Feshbach resonance, as described by the model (1) in the main text, using different theoretical approaches. While in Fig. 1(a) we show $A(\omega)$ as obtained from a single-particle expansion using the time-dependent variational state Eq. (8) of the main text, Fig. 1(b) shows the result using a self-consistent field-theoretical T-matrix approach [1]. Finally the results are compared with Fig. 1(c) which shows the result from the time-dependent coherent state approach as described by Eq. (3) in the main text. All results are obtained for $a_{BB} = 0$ and a cutoff scale $n^{-1/3}\Lambda = 20$. We note that the result shown in Fig. 1(a) has been obtained previously in Ref. [1] using a non-self-consistent T-matrix (NSCT) approach which is equivalent to the time-dependent single particle excitation ansatz Eq. (8) when $a_{BB} = 0$.

The main features in the NSCT/single particle excitation approach are the coherent polaron excitations at negative and positive energies. In this approach the attractive polaron peak exists at arbitrary interaction strength, and the excitation follows the mean-field prediction $E_{MF} = -\frac{2\pi}{\mu_{\rm red}} n a_{IB}$

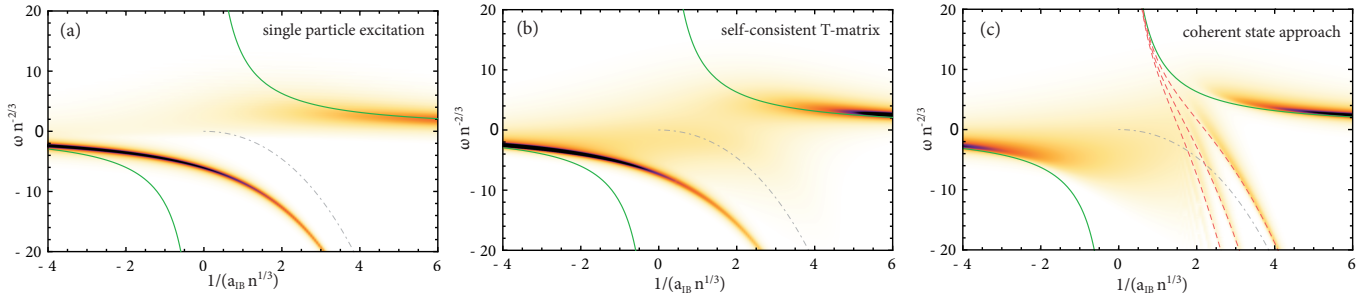

Figure 1. Comparison of the polaron excitation spectrum as function of frequency and inverse interaction strength as obtained from various theoretical approaches. (a) Time dependent single-particle excitation ansatz (which is equivalent to a non-selfconsistent T-matrix approach previously obtained in [1]); (b) self-consistent T-matrix approach; (c) time-dependent mean-field/coherent state approach as described in the main body of the text. The results are obtained for a Bose gas with $a_{BB} = 0$ and the range of the impurity-bath interaction is set by the UV cutoff scale $n^{-1/3}\Lambda = 20$. As in Fig. (1) of the main text the green line shows the saddle point prediction Eq. (4) for the polaron energy while the gray lines give the two-body dimer binding energy. Finally the red dashed lines in (c) show the energies of the high-order phonon-impurity bound states.

(green line) in the limit of small dimensionless interaction parameter $n^{1/3}|a_{IB}| \ll 1$. As the Feshbach resonance is crossed to positive $1/(n^{1/3}a_{\rm IB})$ the attractive polaron peak looses weight. However, in contrast to the coherent state approach [cf. Fig. 1(c)], neither the destruction of the polaron quasiparticle at resonance is captured, nor the formation of the series of bound states for increasing $1/(n^{1/3}a_{\rm IB})$. At positive scattering length a_{IB} the repulsive polaron excitation at positive energies is recovered. It follows the saddle point prediction only for very weak effective impurity bath interactions.

Away from the coherent excitations, the NSCT/single-particle excitation approach predicts a spectral gap between the attractive polaron and zero energy, cf. Fig. 1(a). This gap is, however, an artifact of the approximation. For instance, in a self-consistent T-matrix (SCT) approach, shown in Fig. 1(b), such a gap is absent. In this approach an infinite number of particle excitations is taken into account at the basis of a self-consistent calculation of the in-medium T-matrix and impurity self-energy (the computational details are described in [1]). The, compared to the NSCT approach, increased number of bosonic excitations leads to an additional renormalization of the spectrum. As one consequence the spectral gap, visible in the NSCT approach, is absent and furthermore the repulsive polaron looses additional spectral weight as the Feshbach resonance is approached from the side of negative scattering length. This loss of spectral weight is even more pronounced in the coherent state approach, cf. Fig. 1(c), where multiple boson fluctuations lead to the destruction of the attractive polaron peak.

In contrast to the coherent state approach, the single-particle excitation and SCT approaches do not describe the formation of the series of bound states. In the case of the single-particle excitation approach this fact is simply explained since only one boson excitation is allowed in the wave function. The SCT approach, which allows in principle more than one bosonic excitation, yet does not reveal higher order bound states. We attribute this fact to the specific momentum

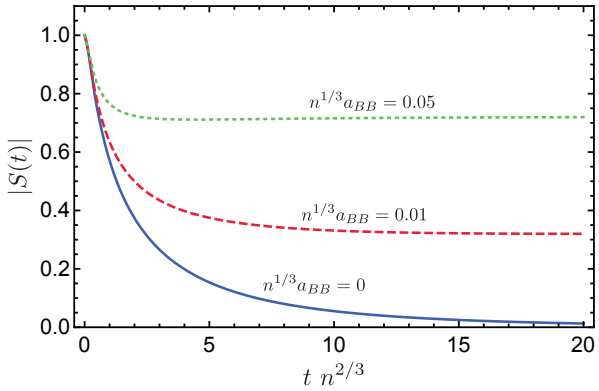

Figure 2. Absolute value of the time dependent overlap $S(t)$ of a single impurity immersed in a BEC as a function of time shown for three Bose scattering lengths. The result is shown for a momentum cutoff $\Lambda n^{-1/3} = 20$, mass-balanced system $m_I = m_B$, and inter-species scattering length $1/(n^{1/3}a_{\rm IB}) = -3$.

structure generated by the SCT approach which only allows for fluctuations in the pairing channel of the interaction vertex. The particular correlations captured by this momentum structure seems to be insufficient for a description of the multiple bound state formation. Finally we note that both the SCT and the coherent state approach show a more pronounced repulsive polaron peak as compared to the single-particle excitation approach which can be tested by radio-frequency spectroscopy of impurities immersed in a BEC of ultracold atoms.

Our results also demonstrate a particular strength of real-time methods: We find that the quasi-particle weight, as determined by $|S(t \to \infty)|$, is strongly dependent on the Bose-Bose interaction strength, as illustrated in Fig. 2. For vanishing Bose-Bose interactions the gas is arbitrarily compressible allowing for strong density variations in the cloud. This is reflected in the quasiparticle weight approaching zero even for rather weak attraction between the impurity and bosons.

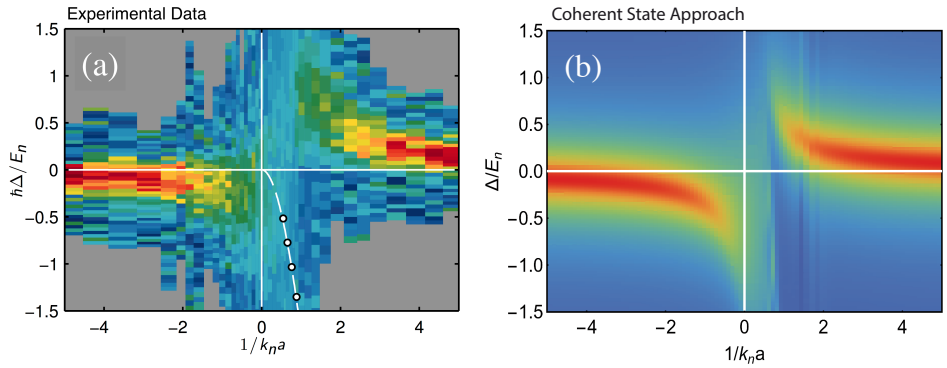

Figure 3. Comparison of the polaron excitation spectrum as function of dimensionless detuning frequency ($E_n = \hbar^2 k_n^2/2m_B$) and inverse interaction strength observed experimentally as presented in [3] (panel a) and predicted with time-dependent coherent state approach (panel b). The experimental signal strength is normalized for each $(k_n a_{IB})^{-1}$ such that it obeys the spectral sum rule for each interaction strength, as intrinsically valid for the theoretical prediction.

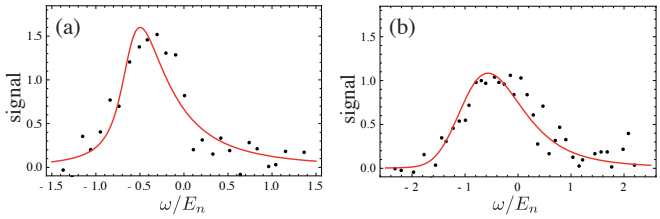

Figure 4. Comparison of the signal amplitude as a function of the detuning near the resonance for two interaction strength: (a) $(a_{IB}k_n)^{-1} = -0.62$, (b) $(a_{IB}k_n)^{-1} = -0.04$. The experimental data [3] and our prediction are shown as black dots and solid red lines, respectively. For our theoretical data we use a length of the RF pulse $\tau_{\rm RF} n^{2/3} = 0.8$. The signal strength is given in arbitrary units.

The polaron formation is only stabilized for sufficient Bose-Bose interactions. This effect cannot be easily seen just from the calculation of the absorption spectrum. This again shows the striking difference between few excitation expansions and the coherent state approach, since the quasiparticle weight is strongly dependent on the number of excitations. The few-particle excitation expansions (one-, two-, ...) allow only a few phonons to be excited from the Bogoliubov vacuum and thus they dramatically overestimate the quasiparticle weight.

V. COMPARISON WITH EXPERIMENT

During the submission process the first experimental observations of attractive and repulsive polarons in a Bose-Einstein condensate has been reported by the group of J. Arlt in Aarhus [3] and groups of E. Cornell and D. Jin at JILA [4]. In this section we briefly discuss the comparison of our theoretical predictions to the experimental data. To make the comparison we repeat our calculations using parameters as realized in the experimental setups.

Aarhus experiment

We provide a comparison between our theoretical prediction and the experimental observation of the repulsive and attractive polaron branches [3]. The experimental measurements were performed for a mass balanced system $m_B = m_I$ using different hyperfine states of ^{39}K atoms. The BEC of the ^{39}K atoms is weakly interacting with the strength $k_n a_{BB} \approx 0.01$, where k_n is fixed by the average inter-particle distance $k_n = (6\pi^2 n)^{1/3}$.

Fig. 3 shows the RF absorption spectra of the impurities observed in experiment (panel a) and calculated within the time-dependent coherent state approach (panel b). The experimental results are in excellent quantitative agreement with our theoretical predictions. For instance, the comparison shows that the positions of the repulsive and attractive polaron branches are predicted with high accuracy. Moreover, our theoretical approach captures correctly the spectral broadening in the strong coupling regime close to the Feshbach resonance. As described in the main body of the text we attribute this effect to the breakdown of the quasiparticle picture due to the excitation of a large number of low-energy Bogoliubov excitations which is captured by our approach. The absence of coherent excitations in the strong coupling regime is further demonstrated in Fig. 4. Here we show the signal amplitude as a function of the detuning near the resonance for two interaction strengths. In Fig. 4(a) the spectrum is shown for a fixed interaction strength $(a_{IB}k_n)^{-1} = -0.62$, and in Fig. 4(b) for close-resonant interactions, $(a_{IB}k_n)^{-1} = -0.04$. In our comparison we account for the non-zero Fourier width of the RF probe. When calculating the Fourier transform of the time-dependent overlap we use an exponential decay $\exp(-t/\tau_{\rm RF})$ with the time $\tau_{\rm RF}$ corresponding to the length of the RF signal

$$A(\omega) = \int dt S(t) e^{-t/\tau_{\rm RF}} e^{-i\omega t}.$$

This leads to the broadening of the polaron branches in the weak coupling regime as well as for the bound state peaks

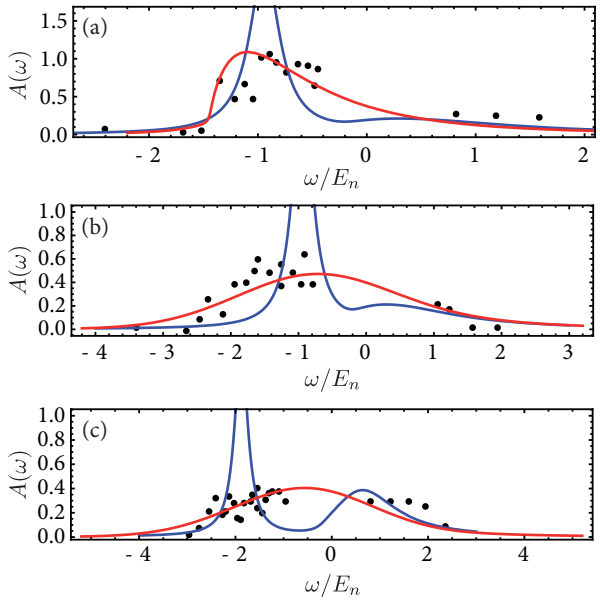

Figure 5. Comparison of the absorbtion spectra $A(\omega)$ as a function of the detuning frequency ω near the resonance for several interaction strengths: (a) $(a_{IB}k_n)^{-1} = -0.25$, (b) $(a_{IB}k_n)^{-1} = 0.18$, (c) $(a_{IB}k_n)^{-1} = 0.3$. The experimental data [4] and the prediction from our approach are shown as black dots and solid red lines, respectively. For comparison the prediction from the single excitation expansion is given by the blue lines.

close to the Feshbach resonance. We expect that the many-particle bound state peaks will be smeared out upon the inclusion of trap averaging. However, with the use of flat trap potentials the observation those spectral feature can be resolved with higher precision [5]. Note that while in the weak coupling regime the width of the signal depends strongly on the pulse duration (for Fig. 3 and Fig. 4 we choose $\tau_{\rm RF} n^{2/3} = 0.8$), in the strong coupling regime we find that broadening of the signal is intrinsic and independent on an additional Fourier spectral broadening.

JILA experiment

We provide a comparison between our theory and the recent experiment on impurities interacting with a BEC of ultracold atoms in the strong coupling regime [4]. In this experiment the absorption spectra of ^{40}K impurities interacting with a BEC of ^{87}Rb atoms has been measured using RF spectroscopy.

In Fig. 5 we compare our theoretical prediction for the absorption spectra with the result of the experiment near the Feshbach resonance for several inter-species scattering lengths. For the comparison we also plot the prediction of the single-excitation expansion used by authors in [4] for interpreting their results, in terms of the energy of the polaron branches, away from the Feshbach resonance. Our theoretical prediction based on the coherent states approach (red lines) has no fitting parameters and is in excellent agreement with experimental data on both sides of the Feshbach resonance.

In contrast to the single particle excitation expansion (blue lines), our method predicts a very broad spectral feature and no sharp peak, which would correspond to a polaron quasiparticle, can be assigned to the spectrum. As we mentioned in the main text of our manuscript, this is the signature of the breakdown of the quasiparticle picture, which is the result of the interplay between few- and many-body correlations. This effect cannot be captured by few particle excitation expansions above the vacuum state to any finite order, since it requires a large number of phonons excited from the BEC state.

[1] S. P. Rath and R. Schmidt, Phys. Rev. A **88**, 053632 (2013).

[2] L. P. Pitaevskii and S. Stringari, *Bose-Einstein Condensation* (Oxford: Clarendon, 2003).

[3] N. B. Jørgensen, L. Wacker, K. T. Skalmstang, M. M. Parish, J. Levinsen, R. S. Christensen, G. M. Bruun, and J. J. Arlt, ArXiv e-prints (2016), arXiv:1604.07883 [cond-mat.quant-gas].

[4] M.-G. Hu, M. J. Van de Graaff, D. Kedar, J. P. Corson, E. A. Cornell, and D. S. Jin, arXiv:1605.00729 (2016).

[5] N. Navon, A. L. Gaunt, R. P. Smith, and Z. Hadzibabic, Science **347**, 167 (2015), http://science.sciencemag.org/content/347/6218/167.full.pdf.